ISTITUTO NAZIONALE DI FISICA NUCLEARE

Sezione di Frascati

**INFN/21-01-LNF**
**29 April 2021**

# PROPOSAL FOR THE REUSE OF THE ELI-NP GBS PRE INJECTOR FOR A RADIOACTIVE BEAMS FACILITY

Alessandro Variola [1], David Alesini [2], Kevin Cassou [3], Kevin Dupraz [3], Franck Falcoz [4] ,Antonio Falone [2],Anna Giribono [2], Aurelien Martens [3], Stefano Pioli [2], Jessica Scifo [2], Cristina Vaccarezza [2], Fabian Zomer [3]

[1)] *INFN-Roma1, Piazzale Aldo Moro,2 00161 Rome, Italy*

[2)] *INFN-LNF, Via Enrico Fermi,40 00044 Frascati Rome, Italy*

[3)] *CNRS In2P3, IJCLab Orsay, France*

[4)] *Amplitude Systems, Pessac, France*

**Abstract**

In the framework of the ELI-NP GBS program a full pre-injector was delivered in the Magurele premises (Romania). This article develops the scenario of the re-use of the pre injector components to integrate a radioactive beams facility in the ELI site, considering the possible interest of the local nuclear physics community.

*Published by*
*Laboratori Nazionali di Frascati*

## 1 Introduction

The ELI-NP project was established looking at its scientific potentials in the field of Nuclear Physics and Nuclear Photonics thanks to an high intensity laser system (up to $10^{24}$ W/cm$^2$) joined with a high brilliance Gamma ray Beam System. The latter, based on a Compton Backscattering Sources (CBS) [1] was meant to provide a photon beam to provide a source with unprecedented quality in terms of small bandwidth (0.5 $\%$), very high spectral density ($> 10^4$ photons/sec/eV) and peak brilliance ($>10^{21}$) in the wide energy range 0.2 - 19.5 MeV. At present a major deadlock situation appeared and a new scenario has to be explored. In this framework it has been proposed the possibility to reuse the quasi totality of the pre-injector of the ELI-NP GBS source to integrate a radioactive beams facility in Magurele. This idea was the optimal compromise found once different constraints was taken into account: a) the new proposal should not be a Compton Gamma Source b) the new project should maximize the interest in the Romanian scientific community c) the performance of the new project should represent an added value in its present scientific context d) the maximum part of the ELI NP GBS pre-injector elements has to be used and extra modifications has to be minimized e) the new project must be reliable and robust to decrease the associated risks. The ALTO facility [2] of the IJCLab Orsay was taken into account as reference to explore the possibility to extend the physical parameters of the accelerators for the new configuration. In this framework the ALTO linac is operated with a repetition frequency of 100 Hz, exactly the same of the ELI NP GBS RF power systems, a variable pulse length and an average current of 10 $\mu A$. The last parameter represent the real challenge for a facility designed taking into account the above mentioned constraints. In fact the ELI source was intended to work as a very brilliant source were both the 6D emittance an the average current aspects were optimized. In the new configuration a new design of the photoinjector has to be produced, where it is necessary to increase the average current of a factor 10 (at least) to reach the ALTO intensity. On the other side the beam emittance and energy spread requirements can be mitigated (up to 10 times larger) in respect to the ELI-NP GBS case, giving so different design knobs to obtain the desired result. The new design of a high current photo injector is itself a very interesting aspects for the particle accelerator community. It is worth to mention that the current design of the ELI-NP gamma beam system is flexible enough to accommodate the required upgrade in order to increase the average beam current. From engineering and integration perspective this will require minor modifications with respect to the current configuration. The existing injector is composed by a radiofrequency photo electron gun, two accelerating sections in S-Band and one accelerating section in C-Band. The C-Band section is also provided with special absorbers in order to dump the HOM induced by the beam itself that migth cause emittance degradation or even beam break up. The hardware already produced includes also all the ancillary equipment needed for the functioning of the machine, such as: magnets and power supplies, beam diagnostics and instrumentation, control system, RF power stations and distribution, synchronization and

LLRF system. Although the reuse of such equipment is certainly a remarkable advantage in the development of the machine, it is important to highlight that a re-engineering of all utilities, connections and interface will be needed. This a special topic that will be addressed in the design phase and it is strictly correlated with the final location of the facility. Therefore, a part of some important technological development which are described in the next paragraphs, a significant effort must be allocated to the integration of the machine itself which includes also radioprotection issues that are quite important especially for a high current radio-active beam facility. Hereafter the first preliminary analysis and considerations on this facility feasibility are summarized.

## 2 Beam Optics

Beam dynamics studies have been performed to provide a reliable working point for the linac to drive in collision with the laser pulse a 3 nC electron beam with 1 mm transverse spot size. The study starts from the layout of the ELI-NP GBS machine and from the considerations on the beam dynamics reported in [1]. A 3 nC electron beam with a final energy of 170 MeV, 1.7 mm length and 9 mm-mrad normalised emittance is delivered at the interaction with a counter-propagating laser pulse. The beam is generated in the ELI-NP GBS photoinjector consisting of an S-band RF photo-gun, equipped with an emittance compensation solenoid, followed by two S-band accelerating structures; the downstream C-band linac, consisting in one single accelerating structure, delivers the beam at the Interaction Point (IP). A quadrupole triplet provides a flexible final focusing for matching the electron beam spot size to the counter-propagating laser pulse.

Regarding the beam dynamics simulations, the machine can be split into two parts with the beam crossing two different regimes: the laminar regime in the photoinjector, where the beam dynamics optimisation is mainly devoted to minimise the space-charge induced emittance, and the emittance-dominated regime, where the total normalised emittance remains constant in an ideal accelerator. This is effective in the C-band booster linac in order to gain energy and manipulate the beam phase space as needed. The photoinjector has been simulated with the multi-particles code ASTRA [3], which takes into account the space charge effects, relevant at very low energies, and the beam intrinsic emittance while the downstream linac has been simulated with the Elegant code [4], that includes the wakefields generated by the electron beam inside the accelerating structures together with the longitudinal space charge and the coherent and incoherent synchrotron radiation effects in the bending magnets. The photoinjector is operated on crest, according to the invariant envelope criteria, aiming to preserve the beam transverse normalised emittance [5][6]. The decision to operate the accelerator in the the range of the nC beam charge has led to adopt a semiconducting cathode, instead of a metallic one as already foreseen at ELI-NP GBS. The main impact of this choice, as extensively reported in paragraph (1.1), limits the RF gun accelerating field amplitude at the cathode whose maximum should not overcome the 100 MV/m value. The beam dynamics has been studies for a gun peak field

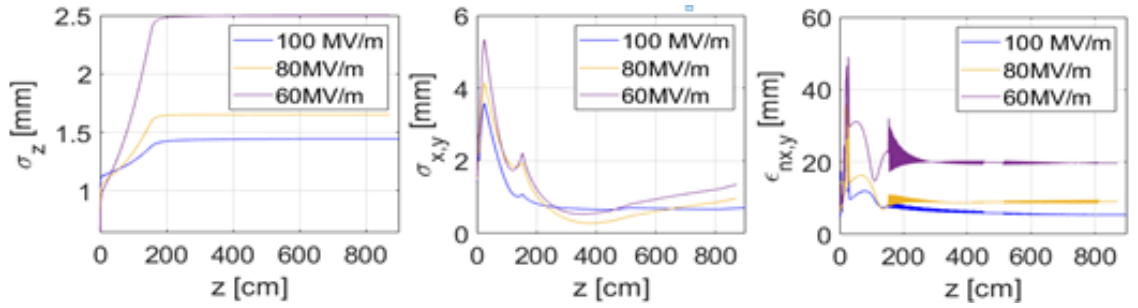


Figure 1: Evolution of the beam parameters from the cathode up to the C-band cavity entrance as obtained by ASTRA simulations for various gun peak field at cathode, Q=3 nC case.

at the cathode varying in the range [60 -100] MV/m as reported in fig.1; the following S-band structures operate at maximum 20 MV/m and the C-band accelerating structure at maximum 25 MV/m, together with the proper off crest operation, i.e. dephasing of about 15 degrees with respect to the maximum RF accelerating field, so to allow to reach 1 $\%$ energy spread at the IP. The final focusing system provides a spot size of $\sigma_{xy}$ = 1 mm. The simulation results are shown in fig.1 and 2. The resulting electron beam parameters at the IP, for a 80 MV/m peak field at the cathode, results to be: $< E >$ = 167 MeV, $\epsilon_{nxy}$ = 9 mm mrad, $\sigma_{xy}$ = 1 mm, $\sigma_E / < E >$ = 1.0 $\%$, $\sigma_z$ = 1.7 mm. In addition, the case of a 6 nC beam charge has been explored with promising results. The photoinjector is operated in the on-crest configuration adopting the same procedure illustrated for the 3nC charge case. The main difference lies in the choice of the gun peak field since, having doubled the beam charge, the space charge forces are now stronger. As one knows, in order to extract the required charge from the cathode, the accelerating field must overcome the beam density field. So, lowering the peak field beyond 80 MV/m, to take into account the space charge effects would lead to laser pulse shaping that could be limited in transverse and longitudinal dimensions by the gun physical dimensions and RF period length. This should result in too much severe downgrade of the accelerator performances. Keeping it in mind, the 80 MV/m value is suggested as minimum peak field for the 6 nC beam. The fig.3 shows the transverse beam size evolution along the photoinjector for 3 and 6 nC charge at 60 and 80 MV/m peak field: for the 6 nC case one can observe a considerable increasing of the beam size in the gun region even using an 80 MV/m peak field, but still avoiding the beam for exploring radial non linearities of the fields. The simulation results for the 6 nC case are shown in fig.4. The resulting electron beam parameters at the IP, for a 80 MV/m peak field at the cathode, results to be: $< E >$ = 167 MeV, $\epsilon_{nxy}$ =20 mm mrad, $\sigma_{xy}$ = 1 mm, $\sigma_E / < E >$ = 2.0 $\%$, $\sigma_z$= 2.35 mm.

## 3 Cs2Te photo-cathodes for The ELI-NP new project

To satisfy the ELI-NP new project requested parameters it is necessary to use semiconductor cathodes. Based on the results so far obtained worldwide in different laboratories,

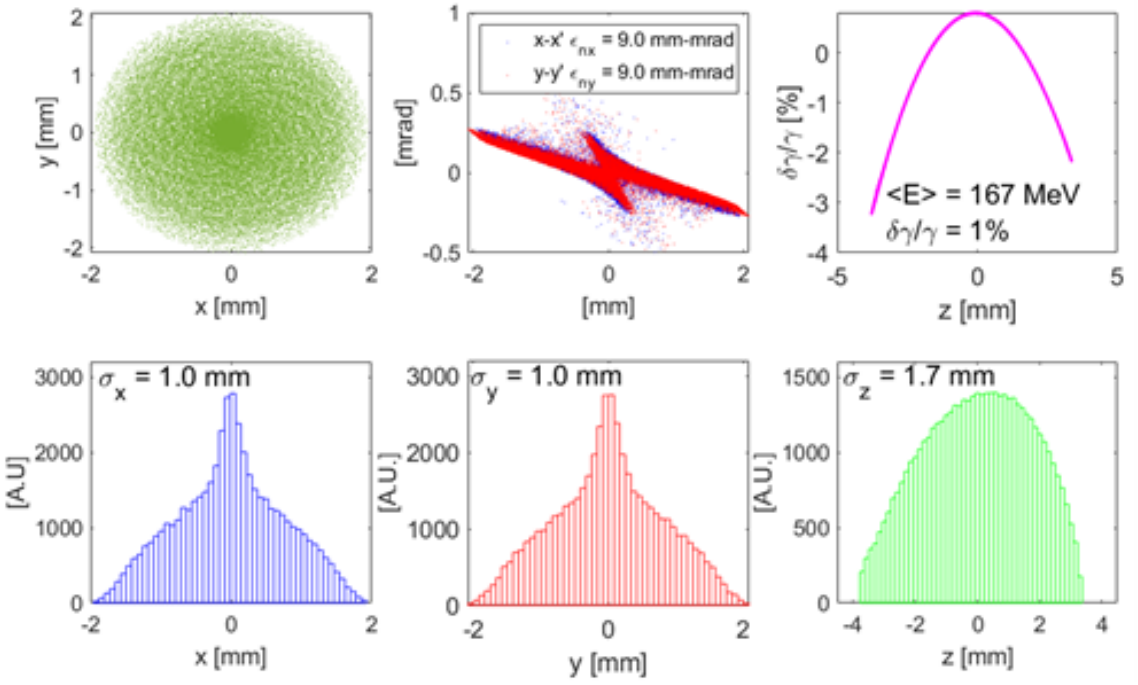


Figure 2: Transverse and longitudinal phase space and distributions at IP for the 170 MeV electron beam as obtained by Elegant simulations, Q=3 nC case.

the most promising semiconductor candidate that can be used as source for electron beam is cesium telluride (Cs2Te) [7],[8]. One of the parameters that is critical for the final choice and operation of the photo-cathode is represented by the Quantum Efficiency (QE) at the drive laser wavelength (UV). Typical QE values for the Cs2Te are about 10% but, due to its low robustness, this value degrades to few percent in few months-years. In this case it is important to have a photo-cathode with the suitable layer thickness of Cs2Te on substrate[9][8]. In terms of intrinsic emittance, at the accelerating peak field of 60 MV/m, its value is $\epsilon_{(n,int)}$=0.96$\mu m/mm$. By using the same accelerating peak field, the QE value is still about 10 %. The Cs2Te photo-cathode demands very good vacuum conditions, at the level of $10^{-10}$ mbar during high gradient operation (max accelerating gradient used to date is about 100 MV/m [7]]), which typically implies that the vacuum without RF be one order of magnitude better in the absence of RF power. These demands are to be met by stringent control of the gun manufacturing and cleaning processes, and by implementing a pumping system with high pumping speed through direct pumping port on the accelerating cells waveguide and cathode flange. Another key point is the essential use of the load lock systems for the RF gun in order to guarantee a fast and safe photo-cathode exchange under vacuum condition. Without the load-lock system, the photo-cathode replacement procedure can take several days and the photo-cathode surface gets contaminated in the atmosphere during installation, leading to undesired QE fluctuation [11]. A proper system must be implemented in the photo-cathode area providing a suitable design for the ELI RF gun. In figure it is reported for reference the SWISS FEL load lock system from the

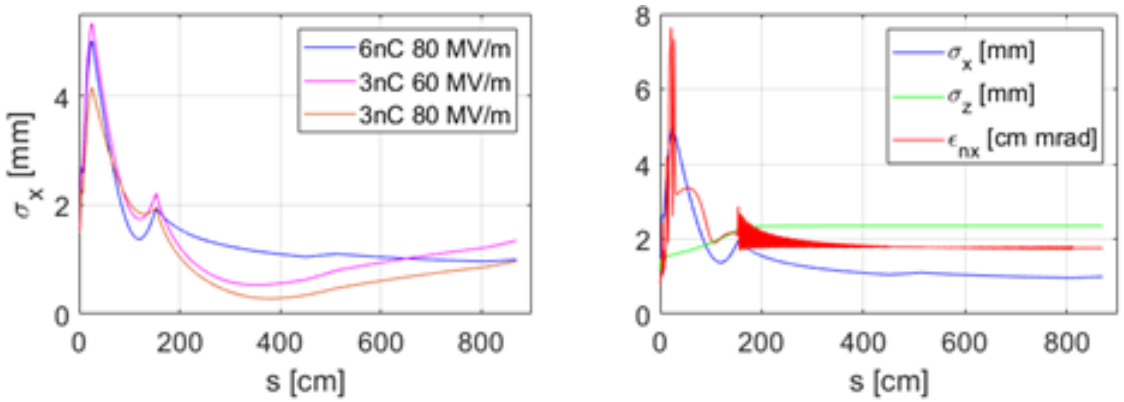


Figure 3: Left: transverse beam size evolution along the photoinjector for 3 and 6 nC charge at 60 and 80 MV/m peak field as obtained by ASTRA simulations. Right: Evolution of the beam parameters from the cathode up to the C-band cavity entrance as obtained by ASTRA simulations for a 6 nC beam and gun peak field at 80 MV/m.

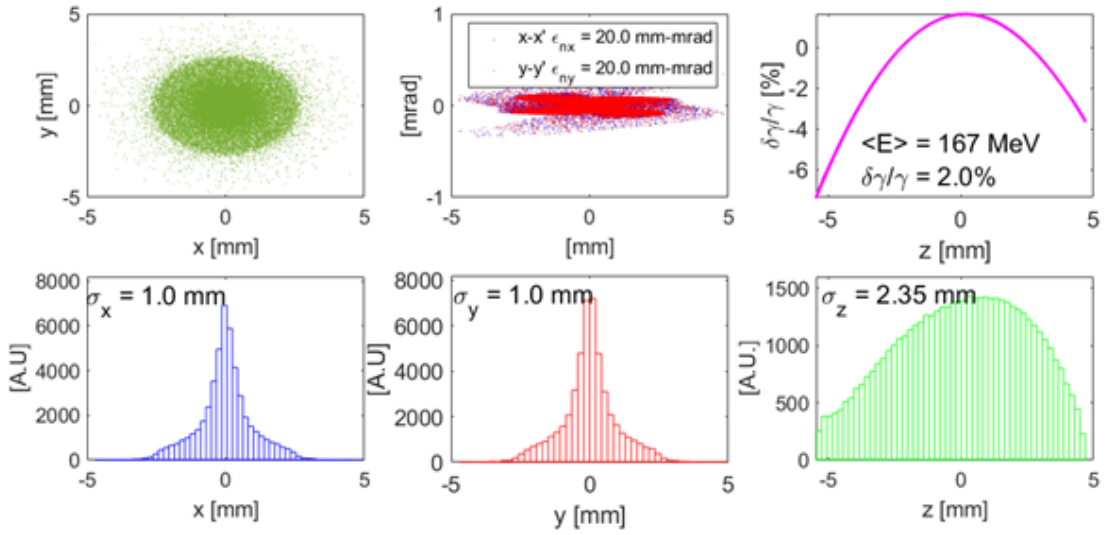


Figure 4: Transverse and longitudinal phase space and distributions at IP for the 6 nC electron beam as obtained by Elegant simulations.

photo-cathode preparation to the RF gun insertion [11].

## 4 Multi-bunch Issues: Beam Loading and Beam Break-up

The passage of electron bunches through accelerating structures excites electromagnetic wakefield. This field can have longitudinal and transverse components and, interacting with subsequent bunches, can affect the longitudinal and the transverse beam dynamics. Those related to the excitation of the fundamental accelerating mode are referred as Beam Loading (BL) effects and can give a modulation of the beam energy along the train while transverse wakefields, can drive an instability along the train called multibunch beam break up (BBU).

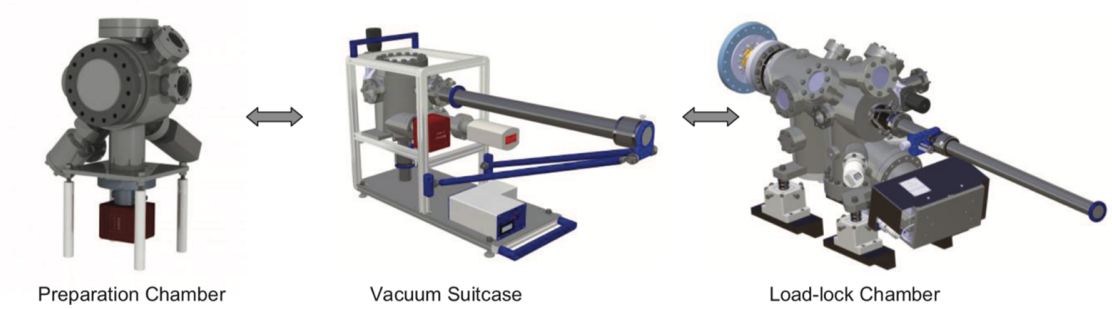


Figure 5: Cathode plugs go first through the preparation chamber (left), are then transported via the vacuum suitcase (center) into the Load-lock chamber (right).

### 4.1 Beam Loading

The main effect of the beam loading is the decrease of the accelerating field gradient in the structure since the effective field can be assumed as a superposition of the RF field and induced wakefield. Several approaches can be found in literature to study and compensate the beam loading effects [12]-[20]. The approaches are different in case of standing wave (SW) structures (like the RF gun) and travelling wave (TW) ones (like the S-Band or C-Band sections).

### 4.2 Beam Loading in the gun

The RF gun is a 1.6 cell RF gun working in S-Band at 2.856 GHz [21]. The main RF parameters are given in Table 1. In the same table we reported the beam parameters used in the calculations of the BL and BBU. If we assume a simple excitation of the gun with a constant RF input pulse, the field in the gun reaches the steady state regime with an exponential behaviour [21]. The final energy spread on the bunch train is then given by the superposition of two contributions: the first given by the exponential behaviour of the accelerating field and the second due to the BL effect. The two contributions are illustrated in fig. 6, assuming that the electron beam is generated in the gun after 1 $\mu s$ with respect to the beginning of the RF pulse. Details of the calculation of the beam loading effects are reported in [21]. To have a uniform accelerating field along the whole bunch train, the input power profile has to be properly shaped as reported in fig. 6 (b). The step profile in the input power allows to have a uniform accelerating field compensating contemporary the cavity filling time effect and the BL one [21].

[1]

[1] As illustrated in the following, the RF input power has a step-like profile to have a constant accelerating field over the bunch train. The two power levels reported in the table are referred to these two levels of power.

Table 1: Parameters of the RF gun and bunch train.

| Parameter | Value |
|---|---|
| Resonant frequency (fres) | 2.856 GHz |
| Cathode peak field (Ecath) | 100 MV/m |
| Ecath/$\sqrt{Pdiss}$ | 37.5 |
| RF input power (Pin) | 11-8.5 MW |
| Filling time ($\tau$) | 460 ns |
| Quality factor (Q0) | 14990 |
| Coupling coefficient ($\beta$) | 2.5 |
| Total RF pulse length | 1.5 $\mu s$ |
| Rep. Rate (frep) | 100 Hz |
| Average diss. power | 900 W |
| Working temperature | 30 $C^o$ |
| Bunch train length | 512 ns |
| Number of bunches | 32 |
| Charge per bunch | 3000 pC |

### 4.3 Beam Loading in the TW structures

A complete discussion on beam loading in TW structures and possible compensation techniques can be found elsewhere in several published papers [13]-[20]. For the ELI linac sections there are two different type of TW cavities: S-Band cavities in the injector and C-Band cavities [22] in the linac booster. The main parameters are reported in Table 2. The beam induced accelerating voltages and the energy spreads due to BL are given in fig. 7 for the two type of structures and for the beam parameters reported in Table 1. Clearly, if not compensated, the BL produces a bunch-to-bunch energy spread along the train well beyond the machine specifications. There are quite a few techniques to compensate these unwanted effects; some of them are based on a proper modulation of the amplitude and phase of the RF input power [15]-[20], others are based on a proper choice of the beam injection time, with respect to the energy filling of the structures. In the present case it is possible to use an amplitude modulation of the input power acting on the low level RF system driving the klystron. The concept takes into account that the structure has to be filled with a proper shaped input pulse, this pre-loads an accelerating field profile equal to the steady-state beam loading one, prior the beam injection. Therefore, since the injection of the very first bunch, the beam experience exactly the steady state beam loading field profile. The details of the full analysis are given in [22] for the C band structures. In fig. 8 we report the final rf input pulses that allow avoiding the BL transient along the train while in fig. 9 the expected bunch energy spread with this compensation, that in both cases is below $\pm 0.1\%$.

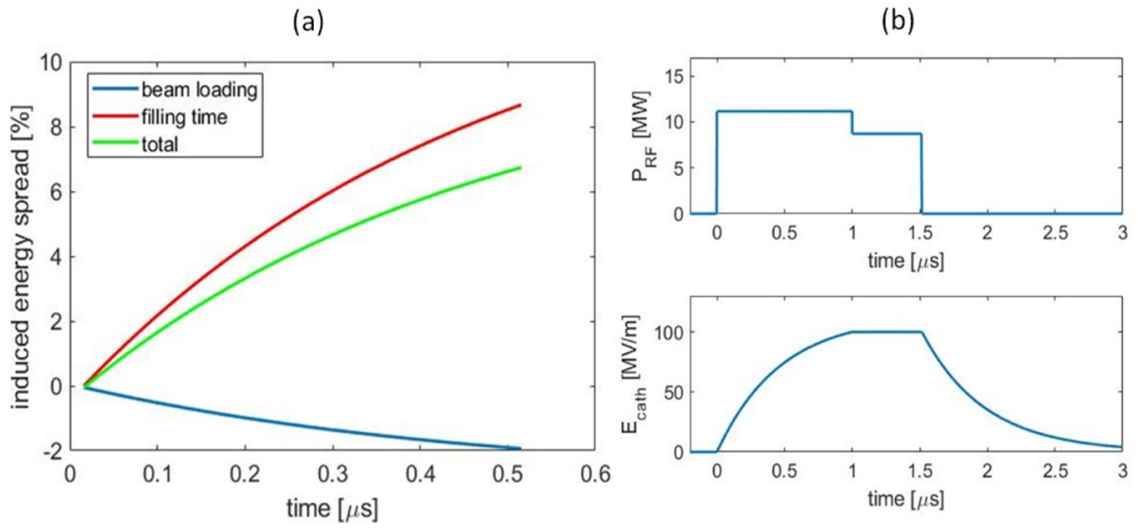


Figure 6: (a) beam induced energy spreads; (b) shaping of the rf input pulse to compensate the induced energy spreads.

### 4.4 Beam Break Up

Of particular concern, in high average current beam dynamics, is the multibunch beam breakup (BBU) driven by the transverse wakefields. As a bunch in the beam train is displaced from the axis, transverse deflecting dipole modes are excited. The trailing bunches are then deflected by the wakefield forces whether they are on axis or not. The angular deflections transform into displacements through the transfer matrices of the focusing system and these displaced bunches will themselves create wakefields in the downstream cavities of the linac. The subsequent bunches will be further deflected leading to an instability growth and beam blowup [23]-[26].

### 4.5 BBU in the C-band LINAC

The C band cavities have been designed to have an effective damping system of the dipole modes [22]. The multi-bunch BBU driven by the transverse wakefields is under control also with the beam parameters reported in Table I that are referred to an average current more than one order of magnitude larger the current foreseen for the ELI-NP working mode. Fig. 10 shows, as an example, the results obtained through a simplified tracking code that shows the increase of the projected emittance as a function of the bunch charge for different average $\beta$-functions and assuming: 1) a 200 $\mu m$ displacement of the whole beam, 2) an injection energy (Ein) in the C band linac of 50 MeV and 3) an output energy Eout=200 MeV. The code considers the first dipole mode in the structure with a quality factor of 100 but assumes, conservatively, a perfect build up mechanism of the instability. This is an extremely conservative assumption.

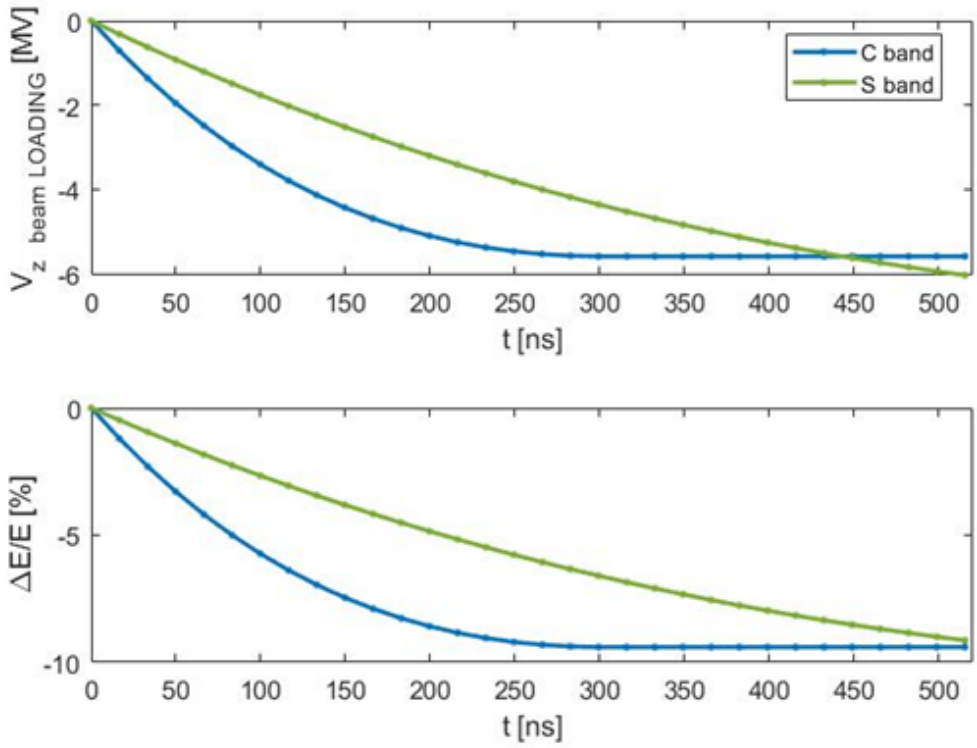


Figure 7: Energy spread induced by BL in the TW structures.

### 4.6 BBU in the S-band TW structures

The TW accelerating structures in the injector are two S-Band travelling wave cavities of the SLAC-type [27]. These cavities are disc loaded structures without damping. A careful analysis of the possible induced BBU instabilities have been done [1]. Even if, in fact, the transverse wakefield per unit length scales with the third power of the working frequency, the beam rigidity in the injector is much lower than in the C band cavities and a transverse voltage induced by the beam can have strong effects in the beam dynamics. The use of S-Band undamped structures was supported even because experimental measurements of induced BBU in S-Band linacs have been done in other experiment [25] and did not put in evidence strong instabilities effects. The analysis of the multi-bunch BBU in the ELI S-Band injector has been performed by using two independent approaches for the transverse wakefield calculation:

1. calculating the dipole modes frequencies and transverse impedances with a mode matching technique and reconstructing the total transverse wakefield by a superposition of the different modes (fig. 11(a));

2. calculating the transverse wakefield of each TW structure by the electromagnetic code GdFidL [28] (fig. 11(b)).

The wakes have been, then, inserted in a simple tracking code and the increase of the projected emittance of all bunches (calculated as Courant Snyder Invariants of macropar-

Table 2: Parameters of the S-Band and C-band TW accelerating structures.

| Parameter | S-Band | C-Band | Unit |
|---|---|---|---|
| Working frequency (fRF) | 2.856 | 5.712 | GHz |
| Number of cells | 84 | 102 | |
| Phase advance per cell | $2\pi/3$ | $2\pi/3$ | |
| Structure length | 3 | 1.8 | m |
| Rep. Rate (frep) | 100 | 100 | Hz |
| Group velocity (vg/c) | 2-0.6 | 2.5-1.5 | % |
| Iris half aperture radius | 13-9.5 | 6.8-5.8 | mm |
| Nominal RF input power (PIN) | 42 | 40 | MW |
| Average accelerating (Eacc) | 23.5 | 33 | MV/m |
| Quality factor (Q) | 12300 | 8800 | |
| Shunt Impedance per unit length (r) | 53 | 70 | MΩ/m |
| Filling time ($\tau F$) | 850 | 320 | ns |
| Field attenuation constant ($\alpha$) | 0.19 | 0.34 | 1/m |
| Average dissipated power @ Eacc | 4.1 | 2.3 | kW |

ticles) at the end of the injector have been calculated for all the bunches. The two different approaches for the wake calculation have advantages and disadvantages. The first one is only an analytical approximated technique based on the mode matching technique, allowing calculating the properties of the single resonant modes while, in principle, GdFidL can give the exact transverse wake of the structure. On the other hand, with the first approach, we can calculate different transverse wakes assuming small errors in the calculated frequencies of the dipole modes and a statistical analysis of BBU can be performed [1]. The transverse wakefield calculated with the analytical approach is given in fig. 11 (a). The corresponding increase of the projected emittance of all bunches at the end of the injector assuming an initial energy (after the gun) of 5 MeV and an energy at the end of the S-Band sections of 80 MeV, are given on fig. 12 (a) assuming an initial error for all bunches at injection of 200 $\mu m$ and an average $\beta$-function of 3 m. The same calculation done with the GdFidL wake gives the results reported in fig. 12 and does not put in evidence a significant increase in the projected emittance. Further calculations can be in principle done but the experimental evidence [14] of a stable accelerated beam with a similar average current foreseen for the ELI case put in evidence that the approach using the mode matching technique is pessimistic.

## 5 Laser System

The ELI-NP Gamma Beam Source was based on the generation of 32 electron bunches. These electron bunches were supposed to be generated by a photocathode laser delivering 32 UV pulses. In the first part of this document we will briefly describes this laser system.

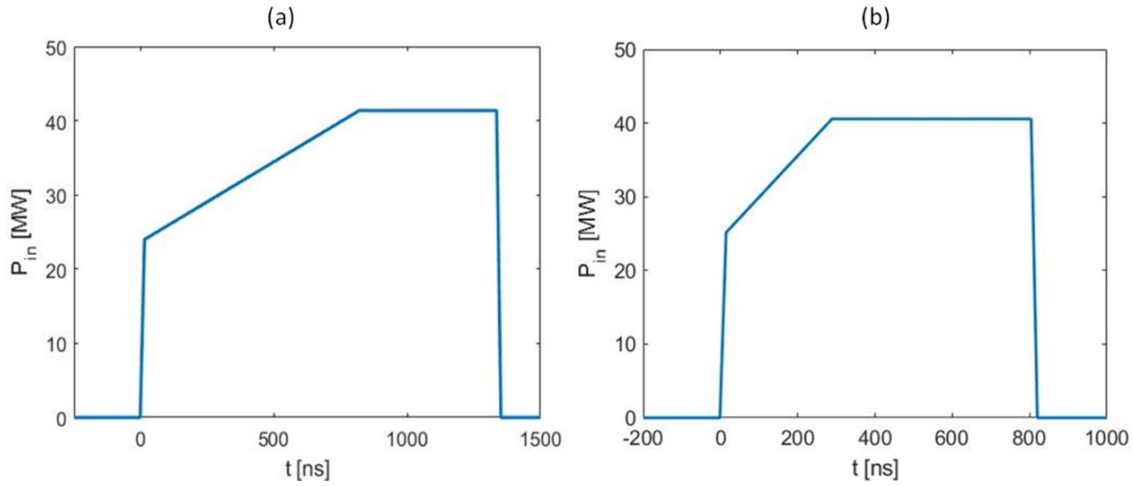


Figure 8: RF input power shaping to compensate the BL effects in S band (a) and C-band TW structures.

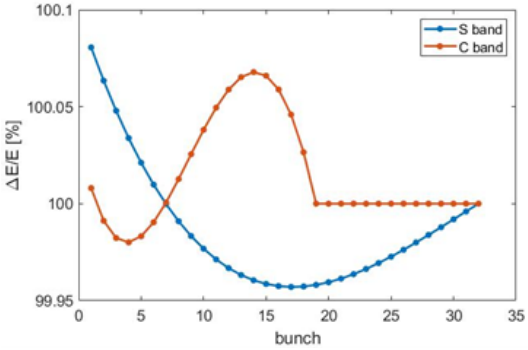


Figure 9: Residual energy spread along the bunch train after BL compensation.

### 5.1 Existing system

The photocathode laser is based on a high energy Ti:Sapphire system working at 100Hz. To generate the 32 pulses a multi-pulse generator (MPG) has been designed and implemented in the system. The goal of this MPG is to 'transfer' the energy from a single pulse to 32 equal pulses that exhibits the same characteristics. The period of this pulse train can be slightly adjusted around 16.1ns. The following layout (fig. 13) shows the different components used in the system:

The system is designed to amplify the pulses generated from the optical master oscillator used in the timing station. After the Menlo oscillator an adjustable delay line is implemented to modify and control the arrival time of the final UV pulse train. Subsequently the laser pulse is sent to a stretcher that narrows the spectrum to 1nm and allows to stretch the time duration from 100fs to around 200ps, to limit the B-integral and optical damages during amplification process. The stretched laser pulse is then amplified in a standard regenerative amplifier up to a few milliJoule Energy level at 100Hz repetition rate. To ensure reliability and efficiency the Ti:Sapphire crystal is pumped by a diode

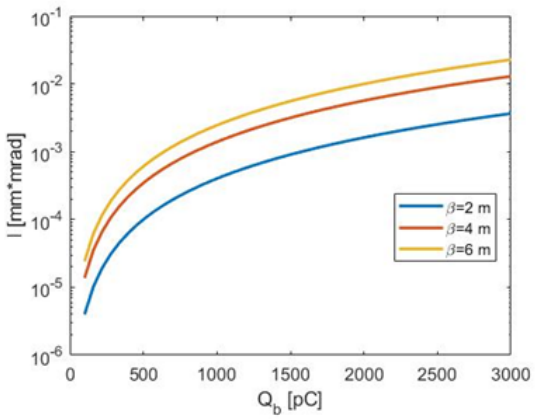


Figure 10: Increase of the projected emittance as a function of the bunch charge for different average $\beta$-functions and assuming a 200 $\mu m$ displacement of the whole beam.

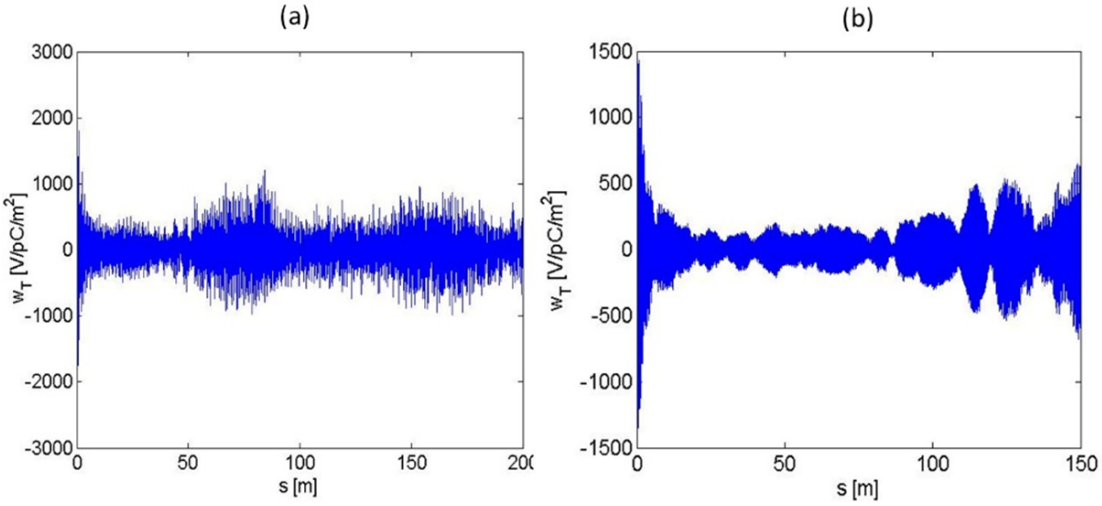


Figure 11: Transverse wakefield in the S band TW structures calculated using the mode matching technique (a) and the GdFidL code (b).

pumped Nd:YAG green laser. A small multi-pass pre-amplifier, also using diode-pumped Nd:YAG green laser, brings the energy level per pulse at 25mJ at 100Hz. The laser system layout is modified from a standard one to implement the MPG system that will generate the train of 32 pulses. The MPG consists of 3 main components:

- A first pulse divider that generates 2 laser pulses of equal energy delayed by 16.1 ns that corresponds to the 46th Harmonic of the machine RF.
- A lossy cavity with a roundtrip period of 32.2 ns (2xRF/46) that produces a decreasing pulse train.
- A Fast Pockels cell with 32 input channels to modulate the pulse to pulse energy in the train. Figure 14 shows the result obtained at the output of the cavity and the Pockels cell.

The pulse train is then sent in the main multipass amplifier to boost the energy to around 5 mJ per pulse. A time-delayed multiplexing of 12 green pump laser is used to

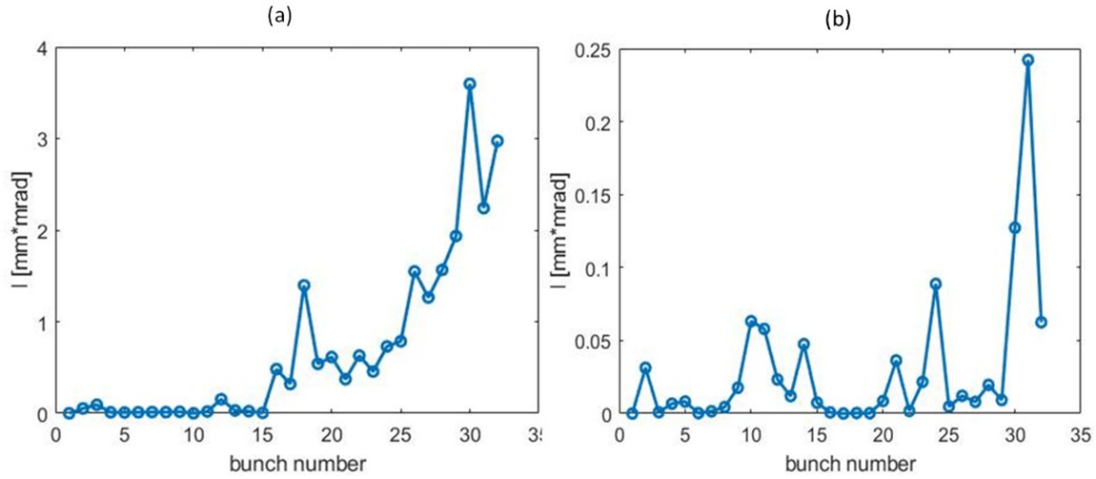


Figure 12: Increase of the projected emittance of all bunches at the exit of the S band injector using the transverse wake given by the mode matching technique (a) and GdFidL code (b).

pump the crystal and allow to flatten the pulse train. Figure 15 shows the output pulse train after amplification.

The pulse train is then compressed down to $\simeq$ 1ps in a double pass reflective dielectric grating compressor in air. The efficiency of the compressor is close to 80%. Two BBO crystal are then used to convert the IR to UV (266 nm) and obtain 32 pulses of 300 $\mu J$.

### 5.2 Possible modifications for the new system

In the new configuration the 32 pulses are not anymore required. To improve the reliability and decrease the complexity of the system it can be interesting to decrease the number of pulses in the train down to 16. This can be easily done by removing the first pulse divider in the MPG, while keeping the rest of the laser chain unchanged. This means that instead of seeding two pulses in the cavity we will inject only one pulses that will generate after 16 round trip the required pulse train. This eliminates the need of a precise alignment system that can ensure the collinearity of two pulses seeded in the cavity. This modification will allow to increase the output energy by a factor close to 2 which is favorable for the new machine. The period between pulses has to be kept to a multiple of 16.1 ns in order for the fast pockels cell to allow the control of the amplitude of each individual pulse.

## 6 Conclusions

In this article the possibility to reuse the ELI NP GBS injector as driver for a radioactive beams facility was explored. Preliminary studies show that new working points exists taking into account the new required performances as far as the beam parameters are concerned. To increase the average current, the gun has to be modify, especially taking

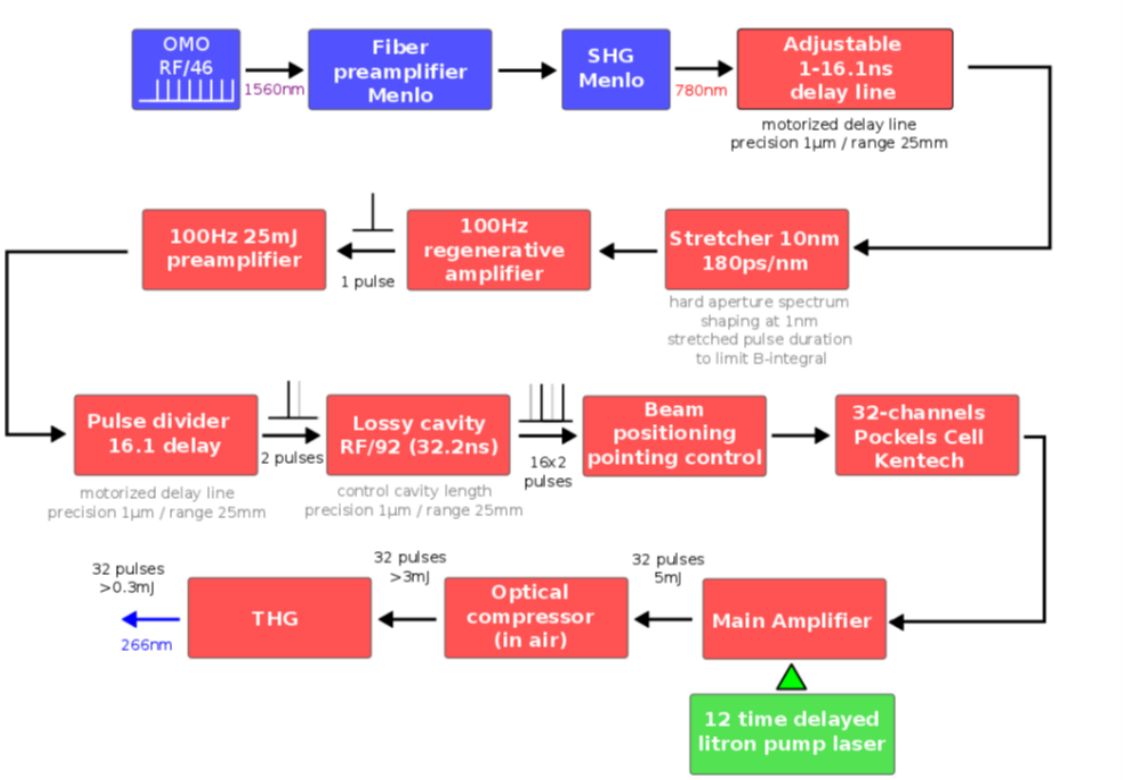


Figure 13: Layout of the laser system

into account a Cs2Te cathode with its load-lock system. Different studies were carried out to demonstrate that both the beam loading and the BBU effects does not represent a limit for the new average current regime. At the end a fast analysis of the possible expected modifications to the PhotoCathode Laser system were illustrated. All these considerations provide a first, preliminary, feasibility validation for the proposed future facility.

## References

[1] O. Adriani *et al*, Technical Design Report EuroGammaS proposal for the ELI-NP Gamma beam System (Sci, Ed. L. Serafini), arXiv:1407.3669 (2014).

[2] https://www.ijclab.in2p3.fr/en/platforms/alto/

[3] K. Floettmann, ASTRA - A Space Charge Tracking Algorithm

[4] M. Borland, Elegant: A flexible sdds-compliant code for accelerator simulation Advanced Photon Source LS-287 (2000).

[5] M. Ferrario *et al*, Experimental demonstration of emittance compensation with velocity bunching, Phys. Rev. Lett.104, 054801 (2010).

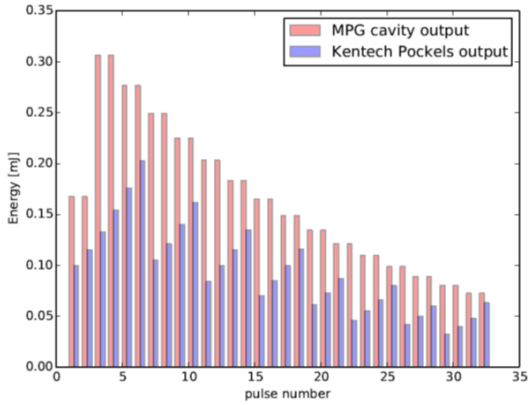


Figure 14: Pulse train output of the cavity and the pockels cells system.

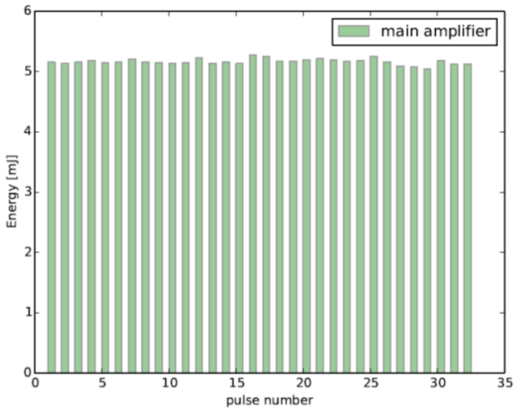


Figure 15: Pulse train output after amplification.

[6] L. Serafini *et al*, Envelope analysis of intense relativistic quasi-laminar beams in rf photoinjectors: A theory of emittance compensation, Phys. Rev., vol. E55, pp. 7565–7590, 1997

[7] E. Prat *et al*, Measurements of copper and cesium telluride cathodes in a radio-frequency photoinjector, Physical Review Special Topics-Accelerators and Beams 18.4 (2015)

[8] Lederer *et al*, Cs2Te Photocathode Lifetime at Flash and European XFEL, Proc. IPAC'18 (2018)

[9] Huang *et al*, Test of Cs2Te Thickness on Cathode Performance at PITZ, 39th Free Electron Laser Conf.(FEL'19), Hamburg, Germany, 26-30 August (2019)

[10] Lederer *et al*, Cs2Te Photocathode Lifetime at Flash and European XFEL, Proc. IPAC'18 (2018)

[11] R. Ganter *et al*, SwissFEL cathode load-lock system, Proc. 35th Int. Free-Electron Laser Conf., New York, NY, USA. (2013)

[12] D. Boussard, Beam loading (particle accelerators), CAS—CERN, Accelerator School: 5th Advanced Accelerator Physics Course, Rhodes, Greece (1993)

[13] J. W. Wang, SLAC Report 339, (1989)

[14] S. Liu *et al*, Nucl. Instrum. Methods Phys. Res. A 584, 1–8 (2008)

[15] C. Adolphsen *et al*, Beam loading compensation in the NLCTA, in proceedings of PAC 97, Vancouver (1997)

[16] A. Lunin *et al*, Phys. Rev. ST. Accel. Beams 14, 052001 (2011)

[17] O. Kononenko and A. Grudiev, Phys. Rev. ST Accel. Beams 14, 111001 (2011)

[18] I. Syratchev and T. Higo, KEK Report 96-8 (1996)

[19] M. Satoh *et al*, Nucl. Instrum. Methods Phys. Res. A 538, 116–126 (2005)

[20] M. Satoh *et al*, Phys. Rev. ST Accel. Beams 12, 013501 (2009).

[21] D. Alesini et al., Phys. Rev. Acc. and Beams 21, 112001 (2018)

[22] D. Alesini et al., Phys. Rev. Acc. and Beams 23, 042001 (2020)

[23] K. Yokoya, DESY Report No. 86-084 (1989)

[24] A. Mosnier, in Instabilities in Linacs, CAS—CERN Accelerator School: 5th Advanced Accelerator Physics Course, Rhodes, Greece, 20 September-1 October 1993, pp. 459–514 (1993)

[25] D. Schulte, in Proceedings of PAC09, Vancouver, BC, Canada FR5RFP055 (2009)

[26] I. Nesmiyan et al., Beam dynamics studies for the CLIC main Linac, Proceedings of IPAC2012, New Orleans, Louisiana, USA, tuppr039 (2012)

[27] R. B. Neal, General Editor, The Stanford Two-Mile Accelerator, W.A. Benjamin, Inc., New York (1968)

[28] www.gdfidl.de